Heliyon 9 (2023) e22503

Contents lists available at ScienceDirect

Heliyon

journal homepage: www.cell.com/heliyon

# Darcy resistant of Soret and Dufour impact of radiative induced magnetic field sutterby fluid flow over stretching cylinder

Nadeem Abbas [a], Zead Mustafa [b], Kamaleldin Abodayeh [a], Taqi A.M. Shatnawi [b], Wasfi Shatanawi [a,b,c,*]

[a] Department of Mathematics and Sciences, College of Humanities and Sciences, Prince Sultan University, Riyadh, 11586, Saudi Arabia
[b] Department of Mathematics, Faculty of Science, The Hashemite University, P.O Box 330127, Zarqa, 13133, Jordan
[c] Department of Medical Research, China Medical University Hospital, China Medical University, Taichung, 40402, Taiwan

A R T I C L E I N F O

*Keywords:*
Sutterby fluid
Induced magnetic field
Stretching cylinder
Radiation
Darcy resistant
Dufour and Soret effect

A B S T R A C T

The incompressible two-dimensional steady flow of Sutterby fluid over a stretching cylinder is taken into account. The magnetic Reynolds number is not deliberated low in the present analysis. Radiation and variable thermal conductivity are considered to debate the impact on the cylindrical surface. The Dufour and Soret impacts are considered on the cylinder. The mathematical model is settled by employing boundary layer approximations in the form of differential equations. The system of differential equations becomes dimensionless using suitable transformations. The dimensionless nonlinear differential equations are solved through a numerical scheme(bvp4c technique). The flow parameters of physical effects on the velocity, temperature, heat transfer rate, and friction between surface and liquid are presented in tabular as well as graphical form. The velocity function declined by improving the values of the Sponginess parameter. The fluid temperature is reduced by increment in curvature parameter.

## 1. Introduction

In the past, several researchers developed ideas using the stretching sheet in two-dimensional flow and heat transfer phenomena, but not much more analysis about the complex problems of the flow over-stretching cylinder. The problem developed having a large radius of the cylinder compared with the thickness of the boundary layer. There are several applications in hot rolling, fiber or wire drawing, and so on. Crane [1] deliberated on the impact of stretching cylinders due to boundary layer flow. Wang [2] debated the stretching cylinder using the fluid flow numerically. Bourgoin et al. [3] premeditated the induced magnetic field flow at the stretching cylinder. Daniel [4] debated the magnetic hydrodynamic steady flow at the porous surface and achieved results analytically. Daniel [5] studied the convective slip of laminar flow at a flat surface and studied the consequences analytically. Daniel [6] considered the magnetic hydrodynamic flow model with slip phenomena at permeable surfaces and solved it analytically. Daniel et al. [7] settled the numerical outcomes of time-dependent magnetic hydrodynamic fluid flow of nanomaterial at the stretchable surface. Meenakumari et al. [8] highlighted the flow impression of chemical reaction with convective Prandtl liquid with induced magnetic field at a stretching surface. Ramamoorthy and Pallavarapu [9] initiated the work on the radiative hall impact for Williamson liquid at the stretching surface. Kotha et al. [10] studied the inspiration of bioconvection laminar flow of nanofluid under the presence of gyrotactic

* Corresponding author. Department of Mathematics and Sciences, College of Humanities and Sciences, Prince Sultan University, Riyadh, 11586, Saudi Arabia.

*E-mail address:* wshatanawi@psu.edu.sa (W. Shatanawi).

https://doi.org/10.1016/j.heliyon.2023.e22503
Received 12 April 2023; Received in revised form 13 November 2023; Accepted 14 November 2023
Available online 19 November 2023
2405-8440/

**Nomenclature**

| | |
|---|---|
| $l$ (m) | Length of stretching sheet |
| $\alpha_f$ $(m^2/s)$ | Thermal diffusivity |
| $(u, v)(m/s)$ | velocity components |
| $b^2$ | Consistency index |
| $T_w$ (K) | Wall temperature |
| $Pr$ (1) | Prandtl number |
| $U_w$ $(m/s)$ | Wall Velocity |
| $Sc(1)$ | Schmidt number |
| $(r$, x)(m) | Coordinates |
| $\gamma_1$ (1) | Curvature parameter |
| $\beta(1)$ | Magnetic field parameter |
| $Rd(1)$ | Thermal radiation |
| $Ec(1)$ | Eckert number |
| $Du$ (1) | Dufour parameter |
| $D_m$ $(m^2/s)$ | Molecular diffusivity of the species concentration |
| $c_s$ | Concentration susceptibility |
| $T_m(K)$ | Mean fluid temperature |
| $Re_x$ (1) | Local Reynold number |
| $\rho(kg/m^3)$ | Fluid density |
| $\tau(J/kgK)$ | Heat capacitance and base fluid ratio |
| $\beta_2(1)$ | Darcy resistant parameter |
| $C_p$ $(J/kgK)$ | Specific heat capacitance |
| $T(K)$ | Prescribed temperature |
| $\nu(m^2/s)$ | Kinematic viscosity |
| $\beta_1(1)$ | Sutterby fluid parameter |
| $k_f$ $(W/m^2K)$ | Thermal conductivity of fluid |
| $T_\infty(K)$ | Ambient temperature |
| $\epsilon(1)$ | Variable thermal conductivity |
| $\lambda_0(1)$ | Magnetic Prandtl number |
| $n$ | Temperature index |
| $Sr$ (1) | Soret parameter |
| $k_t$ | Ratio of thermal diffusion |
| $c_p$(J /kgK) | Heat capacity |
| $q_r$(W $/m^2$) | Radiative heat flux |

microorganisms. The numerical outcomes are debated in their analysis. Gangadhar and Chamkha [11] revealed the impression of a couple stresses of Boussinesq liquid flow under heat generation at a stretchable surface. Meenakumari and Lakshminarayana [12] emphasized the influence of the magnetic hydrodynamic flow of the Powell eyring liquid model using the stretchable surface. Sherma and Wakif [13] comprehensively studied the viscous fluidic media under the convective instabilities. Abbas et al. [14] initiated the influence of non-viscous fluid at the stretching surface. Manzoor et al. [15] worked on the flow of Oldroyd-B nanomaterial fluid under the bioconvective impression. Recently, several authors discussed the boundary layer flow at the stretchable surface under several flow assumptions see Refs. [16–19].

Magnetic field dynamics is the name given to the interaction of a magnetic field with fluid mechanics. The fluids involved in this interaction are referred to as electrically conducting fluids. The dynamics of magnetic field flow drawn the attention of eager scientists from all over the world due to its wide-ranging applications, including astronomical physics, geophysics, and the movement of the earth's layers. The applications of flow problems with magnetic field characteristics in engineering and commercial industry, such as plasma confinement, solar physics, and many more, are also supported by several researchers. The experimental analyst has also noted that when fluid flows are subjected to an external magnetic field, both an electric and magnetic field are generated. Due to the low magnetic Reynold assumption, the induced magnetic field receives most of the energy while the induced electric field is ignored. This generated magnetic field is essential for fluid flow analysis to be accurately represented. The following authors reported preliminary investigations on electrically conducting fluid flows under diverse geometrical situations. Few are mentioned here for the sake of conciseness. Gailitis et al. [20] investigated the influence of induced magnetic field flow using the Riga surface. Mekheimer [21] studied the induced magnetic field flow of peristaltic couple stress liquid at a stretching surface. The effects of pressure gradient, induced magnetic field flow along the axial direction, and temperature gradient are exposed. Daniel et al. [22] highlighted the entropy analysis for magnetic hydrodynamic nanomaterial fluid flow under the impression of radiative chemical reaction and viscous dissipations numerically. Daniel et al. [23] evaluated the flow of MHD using the nanofluid model under mixed convection. Daniel [24] scrutinized the flow of MHD using the nanofluid model under a partial slip impression at a porous surface. Daniel et al. [25] deliberated the flow of MHD using the velocity slip with the nanofluid model under a convective role. Daniel et al. [26] deliberated the time-dependent magnetic hydrodynamic fluid flow of nanomaterial at a stretchable sheet. Daniel et al. [27] considered the thermal stratification flow of magnetic hydrodynamics using the nanofluid model at a stretchable sheet. Mulinti and Pallavarapu [28] considered the flow of UCM fluid under magnetic hydrodynamic and thermal radiation at a porous surface with a chemical reaction. Wakif et al. [29] deliberated an exponentially stretchable surface to analyze the inspiration of MHD and nanofluid. Reddy et al. [30] debated on the Cattaneo-Christov model under Maxwell nanofluid with radiative MHD impression at stretching sheet. Yahaya et al. [31] emphasized the inspiration of magnetic hydrodynamic stagnation region at the stretchable sheet. Scholars have recently deliberated on the influence of the magnetic hydrodynamic model under some assumptions (see Refs. [32–36]).

Applications of the radiative effects in physics and engineering procedures are significant. The temperature processes and space technology heavily rely on the effects of radiation from heat transfer on various flows. However, little is known about how radiation affects the boundary layer. Thermal radiation effects may be a significant problem in the polymer processing sector, as the quality of the completed product depends partly on variables governing heat transport. Daniel and Daniel [37] deliberated the impression of radiative and buoyancy for magnetic hydrodynamic viscous fluid in a porous sheet. They took the results of developing flow problem analytically. Daniel et al. [38] developed the numerical outcomes of radiative and slip influence of nanomaterial liquid flow at porous stretchable surface. Daniel et al. [39] considered the variable thickness of nanomaterial liquid flow at a stretchable sheet. Daniel et al. [40] deliberated the thermal stratification of nanomaterial liquid flow at nonlinear stretchable surface. Daniel et al. [41] reflected the thermal radiation time-dependent flow of nanomaterial fluid at a nonlinear stretchable surface. Gangadhar et al. [42] calculated the couple stress fluid of magnetized flow at a stretchable surface. Reddy and Lakshminarayana [43] worked on the Cattaneo-Christov under Williamson nanofluid with radiative MHD inspiration at stretching sheet. Gangadhar et al. [44] planned the radiation on the flow of Walter's B nanofluid at a rotating surface. Bhargavi et al. [45] debated the radiation for Maxwell hybrid nanofluid. Gangadhar et al. [46] highlighted the impact of the thermal feature of radiative hybrid nanoliquid material flow at rotating cylinder. Recently, researchers have been studied the influence of radiation under several assumptions (see Refs. [47–50]).

From the above literature, the gap of the research available has been filled as sutterby fluid flow over a stretching cylinder in the presence of Dufour and Soret impacts. The induced magnetic field has been considered under the assumption of a high Reynold number. The variable thermal conductivity and radiation impacts have been discussed. Developing a mathematical model under flow assumptions has been considered and solved through the numerical technique bvp4c using MATLAB software. The results have been presented in graphs and tabular form. Such results are unique and have not still discussed before.

## 2. Mathematical formulation

The Darcy resistance flow of Sutterby fluid is considered in this analysis over a stretching cylinder. The flow over the stretching cylinder is presented in Fig. 1. The temperature-dependent flow properties are analyzed at the surface of the cylinder. The radiations are applied using the viscous dissipations of the flow model. The Dufour and Soret impacts are considered on the cylindrical surface. The induced magnetic field is applied along the $r$ direction, which is normal to $x-$ direction. The magnetic Reynolds number is considered large of the induced magnetic field. The stretching velocity of the cylinder is $U_w$, and the temperature of the surface is $T_w$. The ambient fluid temperature and free stream of induced magnetic hydrodynamics are $T_\infty$ and $H_e$. The assumptions of the problem are as follows:

- Induced magnetic field

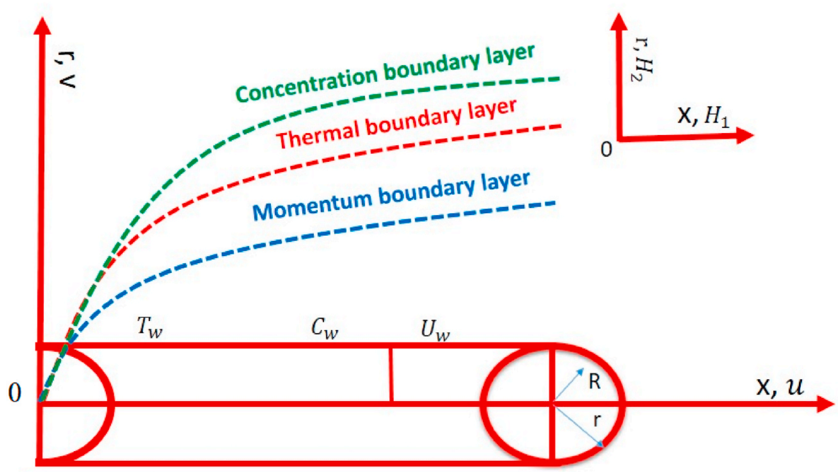


**Fig. 1.** Flow analysis of induced Sutterby fluid over a stretching cylinder.

- Dufour and Soret effects
- Stretching cylinder
- Sutterby fluid flow
- Radiation
- Viscous dissipation and variable thermal conductivity

The governing model is proposed and defined as (see Refs. 28–30,60, 61):

$$\frac{\partial v}{\partial r}+\frac{v}{r}+\frac{\partial u}{\partial x}=0, \tag{1}$$

$$\frac{\partial H_2}{\partial r}+\frac{H_2}{r}+\frac{\partial H_1}{\partial x}=0, \tag{2}$$

$$u\frac{\partial u}{\partial x}+v\frac{\partial v}{\partial r}-\frac{\mu_e}{4\pi\rho_f}\left(H_1\frac{\partial H_1}{\partial x}+H_2\frac{\partial H_1}{\partial r}\right)=\left(\frac{\upsilon_f}{2}\right)\frac{\partial^2 u}{\partial r^2}+\left(\frac{\upsilon_f}{2}\right)\frac{1}{r}\frac{\partial u}{\partial r}-\left(\frac{\upsilon_f ma^2}{4}\right)\left(\frac{\partial u}{\partial r}\right)^2\frac{\partial^2 u}{\partial r^2}+\frac{R_z}{\rho_f}, \tag{3}$$

$$u\frac{\partial H_1}{\partial x}+v\frac{\partial H_1}{\partial r}-H_1\frac{\partial u}{\partial x}-H_2\frac{\partial u}{\partial r}=\eta_0\left(\frac{\partial^2 H_1}{\partial r^2}+\frac{1}{r}\frac{\partial H_1}{\partial r}\right), \tag{4}$$

$$u\frac{\partial T}{\partial x}+v\frac{\partial T}{\partial r}=\frac{1}{\rho c_p}\frac{1}{r}\frac{\partial}{\partial r}\left(rK(T)\frac{\partial T}{\partial r}\right)-\frac{1}{r}\frac{\partial(rq_r)}{\partial r}+\frac{1}{\rho c_p}\left(1-\left(\frac{\upsilon_0 ma^2}{4}\right)\left(\frac{\partial u}{\partial r}\right)^2\right)\left(\frac{\partial u}{\partial r}\right)^2+\frac{D_m k_t}{c_s c_p}\frac{1}{r}\frac{\partial}{\partial r}\left(r\frac{\partial C}{\partial r}\right), \tag{5}$$

$$u\frac{\partial C}{\partial x}+v\frac{\partial C}{\partial r}=D_m\frac{1}{r}\frac{\partial}{\partial r}\left(r\frac{\partial C}{\partial r}\right)+\frac{D_m k_t}{T_m}\frac{1}{r}\frac{\partial}{\partial r}\left(\frac{\partial T}{\partial r}r\right). \tag{6}$$

with BC(boundary conditions):

$$u=U_w=\frac{U_0 x}{l}, v=0, H_1=0, H_2=0, T=T_w, C=C_w, at r\rightarrow R, u\rightarrow 0, H_1\rightarrow H_e, T\rightarrow T_\infty, C\rightarrow C_\infty, as\ r\rightarrow\infty.. \tag{7}$$

The suitable transformations are

$$u=U_w F^{'}(\zeta), v=-\frac{R}{r}\sqrt{\frac{U_0\upsilon_f}{l}}F(\zeta), H_1=\frac{H_0 x}{l}G^{'}(\zeta), H_2=-\frac{RH_0}{r}\sqrt{\frac{\upsilon_f}{lU_0}}G(\zeta), \zeta=\frac{r^2-R^2}{2R}\sqrt{\frac{U_0}{l\upsilon_f}}, T=T_\infty+(T_w-T_\infty)\Theta(\zeta), C=C_\infty + (C_w-C_\infty)\varphi(\zeta).. \tag{8}$$

Using the appropriate transfo rmations and partial differential equations above, we obtain the following ordinary differential equations:

$$(1+2\zeta\gamma_1)\frac{\partial^3 F}{\partial\zeta^3}+2\gamma_1\frac{\partial^2 F}{\partial\zeta^2}+2\frac{\partial^2 F}{\partial\zeta^2}\frac{\partial F}{\partial\zeta}-\left(\frac{\partial F}{\partial\zeta}\right)^2-\frac{\beta_1}{2}(1+2\zeta\gamma_1)\left(\frac{\partial^2 F}{\partial\zeta^2}\right)^2\left((1+2\zeta\gamma_1)\frac{\partial^3 F}{\partial\zeta^3}+\gamma_1\frac{\partial^2 F}{\partial\zeta^2}\right)+\frac{\lambda_1}{2}\frac{\partial F}{\partial\zeta}+\frac{1}{12}\beta_2\left(\frac{\partial^2 F}{\partial\zeta^2}\right)^2\frac{\partial F}{\partial\zeta}+\beta\left(\frac{\partial G}{\partial\zeta}\frac{\partial G}{\partial\zeta} - G(\zeta)\frac{\partial^2 G}{\partial\zeta^2}\right)=0, \tag{9}$$

$$\lambda_0(1+2\zeta\gamma_1)\frac{\partial^3 G}{\partial\zeta^3}+2\lambda_0\gamma_1\frac{\partial^2 G}{\partial\zeta^2}+G(\zeta)\left(\frac{\partial^2 F}{\partial\zeta^2}\right)-\frac{\partial^2 G}{\partial\zeta^2}F(\zeta)=0, \tag{10}$$

$$\frac{1}{Pr}\left(1+\epsilon\Theta(\zeta)+\frac{4}{3}R_d\right)(1+2\zeta\gamma_1)\frac{\partial^2\Theta}{\partial\zeta^2}+\left(PrF(\zeta)+\epsilon(1+2\zeta\gamma_1)\Theta(\zeta)+(1+2\zeta\gamma_1)\frac{4}{3}R_d\gamma_1+2\gamma_1\right)\frac{\partial\Theta}{\partial\zeta}-nPr\Theta(\zeta)\frac{\partial F}{\partial\zeta}+PrEc\left(1 - \frac{\beta_1}{6}F^{''}(\zeta)F^{''}(\zeta)\right)F^{''}(\zeta)F^{''}(\zeta)+Du\left((1+2\zeta\gamma_1)\frac{\partial^2\varphi}{\partial\zeta^2}+2\gamma_1\frac{\partial\varphi}{\partial\zeta}\right)=0, \tag{11}$$

$$(1+2\zeta\gamma_1)\frac{\partial^2\varphi}{\partial\zeta^2}+2\gamma_1\frac{\partial\varphi}{\partial\zeta}+Sc\left(F(\zeta)\frac{\partial\varphi}{\partial\zeta}-n\varphi(\zeta)\frac{\partial F}{\partial\zeta}\right)+ScSr\left((1+2\zeta\gamma_1)\frac{\partial^2\Theta}{\partial\zeta^2}+2\gamma_1\frac{\partial\Theta}{\partial\zeta}\right)=0. \tag{12}$$

with relevant BC(boundary conditions):

$$F(0)=0, (0)=1, F^{'}(\infty)=0, F^{'}(0)=1, \varphi(0)=1, G(0)=0, \Theta(\infty)=0, G^{'}(\infty)=1, G^{'}(0)=0, \varphi(\infty)=0. \tag{13}$$

Where, $\gamma_1$ (Curvature parameter), $\lambda_1$ (Sponginess parameter), $\beta_1$ (Sutterby fluid parameter), $\beta_2$ (Darcy resistant parameter), $R_d$ (Thermal radiation), *Ec* (Eckert number), $\lambda_0$ (Magnetic Prandtl number), $\beta$ (Magnetic field parameter), *Du* (Dufour), *Sr* (Soret), *Sc* (Schmidt) and *Pr* (Prandtl number). Where,

$$\gamma_1\left(\frac{1}{R}\sqrt{\frac{\nu_f l}{U_0}}\right), \beta_1\left(\frac{ma^2 {U_0}^3 x^2}{\nu_f l^3}\right), \beta_2\left(\frac{m^* a^2 {U_0}^2 x^2}{k^* l^2}\right), \lambda_1\left(\frac{\nu_f l}{k^* U_0}\right),$$

$$Sc\left(\frac{\nu_f}{D_B}\right), Ec\left(\frac{{U_0}^2}{c_p(T_w - T_\infty)}\right), R_d\left(\frac{4\sigma^* {T_\infty}^3}{kk^*}\right), Pr\left(\frac{\nu_f}{\alpha}\right),$$

$$Du\left(\frac{D_m k_T(C_w - C_\infty)}{c_p c_s(T_w - T_\infty)}\right), Du\left(\frac{D_m k_T(C_w - C_\infty)}{c_p c_s(T_w - T_\infty)}\right), \lambda_0\left(\frac{\eta_0}{\nu_f}\right) \text{and} \beta\left(\frac{\mu_e}{4\pi\rho_f}\left(\frac{H_0 l}{U_0}\right)^2\right).$$

The coefficients of physical quantities are presented as $C_f$ (Skin friction) and $N_u$ (Heat transfer). The performance of these quantities are well-defined as

$$C_f = \frac{2[\tau_w]_{r=R}}{\rho (U_w)^2}, N_u = \frac{x\left(1+\frac{4}{3}R_d\right)\left[\frac{\partial T}{\partial r}\right]_{r=R}}{k(T-T_w)}, \tau_w = \left(\frac{\partial u}{\partial x}+\frac{\partial v}{\partial r}\right) - \frac{\mu\omega b^2}{12}\left(\frac{\partial u}{\partial x}+\frac{\partial v}{\partial r}\right)\left(2\left(\left(\frac{\partial u}{\partial x}\right)^2+\left(\frac{\partial v}{\partial r}\right)^2+\left(\frac{u}{r}\right)^2\right)+\left(\frac{\partial u}{\partial x}+\frac{\partial v}{\partial r}\right)^2\right). \tag{14}$$

The dimensionless form is presented as

$$ {C_f}^S = \left(\frac{\partial^2 F}{\partial \zeta^2} - \frac{\beta_1}{6}\left[3\left(\frac{\partial F}{\partial \zeta}\right)^2 + 3(1+2\zeta\gamma_1)(F^2) - 2(1+2\zeta\gamma_1)F\frac{\partial F}{\partial \zeta} + (1+2\zeta\gamma_1)\left(\frac{\partial^2 F}{\partial \zeta^2}\right)^2\right]\right)_{\zeta\to 0}, {N_u}^n = -\left(1+\frac{4}{3}R_d\right)\frac{\partial \Theta}{\partial \zeta}_{\zeta\to 0}. \tag{15}$$

## 3. Numerical method procedure

The integral component of solving a BVP is making an initial guess at the solution, and the accuracy of that guess may even determine whether the computation is successful. The boundary conditions define the relationship between the solution values at two points along the interval of integration. The system of differential equations is solved numerical bvp4c technique using the Matlab software package. The numerical procedure of the differential equations is transformed into the first-order differential equations. The selection of finite value is $\zeta\to\infty$ as $\zeta = 10$, which shows that the present results are corrected asymptotically for numerical technique. The $10^{-6}$ is tolerance error of convergence criteria and process is adopted as follows:

$$F(\zeta) = S(1); \frac{\partial^2 F}{\partial \zeta^2} = S(3); \frac{\partial F}{\partial \zeta} = S(2); \frac{\partial^3 F}{\partial \zeta^3} = SS1;\ G(\zeta) = S(4); \frac{\partial^2 G}{\partial \zeta^2} = S(6); \frac{\partial G}{\partial \zeta} = S(5); \frac{\partial^3 G}{\partial \zeta^3} = SS2; ; \Theta(\zeta) = S(7); \frac{\partial \Theta}{\partial \zeta} = S(8); \frac{\partial^2 \Theta}{\partial \zeta^2} = SS3; ; \varphi(\zeta) = S(9); \frac{\partial \varphi}{\partial \zeta} = S(10); \frac{\partial^2 \varphi}{\partial \zeta^2} = SS4; \tag{16}$$

$$SS1 = -\left((1+2\zeta\gamma_1) - \frac{\beta_1}{2}((1+2\zeta\gamma_1))^2(S(3))^2\right)^{-1}\left(2\gamma_1 S(3) - \frac{\lambda_1}{2}S(2) - \frac{\beta_1}{2}(1+2\zeta\gamma_1)(S(3))^2(\gamma_1 S(3)) + \frac{1}{12}\beta_2(S(3))^2 S(2) + \beta(S(5)S(5) - S(1)S(6)) + 2S(3)S(2) - (S(2))^2\right); \tag{17}$$

$$SS2 = -(\lambda_0(1+2\zeta\gamma_1))^{-1}(2\lambda_0\gamma_1 S(6) + S(4)S(3) - S(1)S(6)); \tag{18}$$

$$SS3 = \frac{Pr}{\left(1+\epsilon S(7)+\frac{4}{3}R_d\right)(1+2\zeta\gamma_1)}\left(\left(Pr\, S(1) + \epsilon(1+2\zeta\gamma_1)S(7) + (1+2\zeta\gamma_1)\frac{4}{3}R_d\gamma_1 + 2\gamma_1\right)S(8) - nPrS(7)S(2) + PrEc\left(1 - \frac{\beta_1}{6}S(3)S(3)\right)S(3)S(3) + Du((1+2\zeta\gamma_1)SS4 + 2\gamma_1 S(10))\right); \tag{19}$$

$$SS4 = -((1+2\zeta\gamma_1))^{-1}(2\gamma_1 S(10) + Sc(S(1)S(10) - nS(9)S(2)) + ScSr((1+2\zeta\gamma_1)SS3 + 2\gamma_1(8))); \tag{20}$$

Relevant boundary conditions are

$$S0(1); S_\infty(2); S0(2)-1; S0(4); S_\infty(5)-1; S0(5); S0(7)-1; S0(9)-1; S_\infty(9); S_\infty(7); \tag{21}$$

The interval of integration is divided into smaller intervals by the collocation technique using a mesh points. The boundary conditions and collocation conditions imposed on each subinterval cause a global system of algebraic equations, which the solver solves to produce a numerical solution. The solver then calculates the error of the numerical solution for each subinterval. If the solution doesn't meet the tolerance standards, the solver adapts the mesh and repeats the procedure. A first approximation of the solution at the mesh points must be given along with the initial mesh points. The boundaries of residual are publicized:

$$\widetilde{Y}_1 = |S_2(\infty) - \widehat{S}_2(\infty)|, \widetilde{Y}_2 = |S_5(\infty) - \widehat{S}_5(\infty)|, \widetilde{Y}_3 = |S_7(\infty) - \widehat{S}_7(\infty)|, \widetilde{Y}_3 = |S_9(\infty) - \widehat{S}_9(\infty)|.$$

Here, $\widehat{S}(\infty)$, $\widehat{S_5}(\infty)$, $\widehat{S_7}(\infty)$ and $\widehat{S_7}(\infty)$ are calculated boundary values.

## 4. Results and discussion

The differential equations are interpreted by numerical patterns with the help of MATLAB software packages. The impression of involving physical parameters has been presented through graphs and tabular form. Figs. 2–5 reported the impression Sponginess parameter ($\lambda_1$), Sutterby fluid parameter ($\beta_1$), Darcy resistant parameter ($\beta_2$) and Curvature parameter on the velocity ($F'(\zeta)$). Fig. 2 publicized the variation of the Sponginess parameter and velocity. Velocity declined by improving the values of the Sponginess parameter. Physically, the permeability of the porous material generates a rise in resistance, which lowers the fluid velocity. The fluid velocity and Sutterby fluid parameter variation are offered in Fig. 3 is publicized that fluid velocity deteriorated against the increment in the Sutterby fluid parameter. Because of the increment in the Sutterby fluid parameter, which increment in fluid viscosity, ultimately, fluid velocity declined. The impact of the Darcy resistant parameter indicated the velocity results offered in Fig. 4. The fluid velocity achieved greater when values of the Darcy resistant parameter improved. Fig. 5 is shown the velocity function results for different values of Curvature. The velocity function accelerated for higher values of Curvature. The curvature of the cylindrical surface enhanced, which enhanced fluid velocity. Fig. 6 is revealed the Curvature parameter's impression on the magnetic profile. The curves of the magnetic profile revealed higher than higher for boosting values of the Curvature parameter. The influence of magnetic Prandtl number on the magnetic profile is revealed in Fig. 7. The curves of the magnetic profile publicized higher than higher due to enlarging values of. Figs. 8–12 publicized the effect of Curvature, Prandtl number, Dufour, Eckert number, and radiation on temperature. The impression of temperature and radiation offered in Fig. 8. Temperature revealed larger than larger due to greater values of radiation. The impression of curvature parameter and fluid temperature is publicized in Fig. 9. As the curvature of the cylinder increases, the surface becomes flat, so heat transfer on the surface of the cylinder decreases, and the liquid temperature decreases. The variation of Dufour impact and temperature is publicized in Fig. 10. The temperature enlarged due to augmentation of Dufour parameter because energy flux generation boosted up, which improved the temperature. Fig. 11 shows the variation of fluid temperature and Prandtl factor. Since the Prandtl factor organizes the thickness of the thermosensitive layer, increasing the value of the Prandtl factor decreases the liquid temperature. The impression of Eckert factor and temperature is presented in Fig. 12. The Eckert factor values improved by improving the temperature at the cylindrical surface. Due to the increment in Eckert factor, which boosted up kinetic energy as well as heat transfer enhancement. So, the fluid temperature improved at the surface of the cylinder. Figs. 13–15 debated the influence of Soret, Schmidt, and Dufour on the concentration. Fig. 13 presented the impression of Soret on concentration. The concentration curves revealed declining due to upper values of Soret parameter. Impression of Schmidt factor on the concentration function is stated in Fig. 14. Concentration curves declined due to larger values of Schmidt parameter. Impression of the Dufour parameter on the concentration function is reported in Fig. 15. Concentration curves declined due to larger values of Dufour parameter. Fig. 16 reported the impact of $\epsilon$ on the temperature profile. The temperature boosted due to enlarging values of $\epsilon$. The thermal conductivity values extended ultimately heat transfer phenomena enlarging as well as temperature enlarged.

Table 1 revealed the impression of $\lambda_1$, $\beta_2$, $R_d$ (Thermal radiation), $\epsilon$, $Ec$ (Eckert number), $\lambda_0$ (Magnetic Prandtl number), $\beta$ (Magnetic field parameter), $Pr$ (Prandtl number), $\gamma_1$ (Curvature parameter), $Du$ (Dufour parameter), $Sc$ (Schmidt), $\beta_1$ (Sutterby fluid parameter) and $Sr$ (Soret parameter) on the ${C_f}^S$ and ${N_u}^n$. The heat transfer and friction force revealed lesser than lesser by increment of curvature parameter. The curvature of cylindrical surface expanded and heat transfer phenomena reduced due to large surface area covered. But the skin friction is reduced because increment in curvature of cylindrical surface, the surface becomes flat and friction force is reduced.

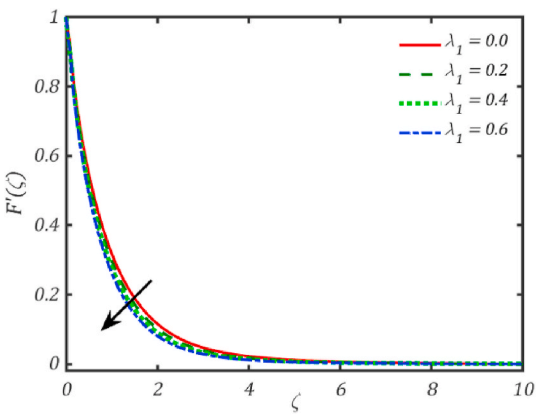


**Fig. 2.** Impression of $\lambda_1$ on $F'(\zeta)$.

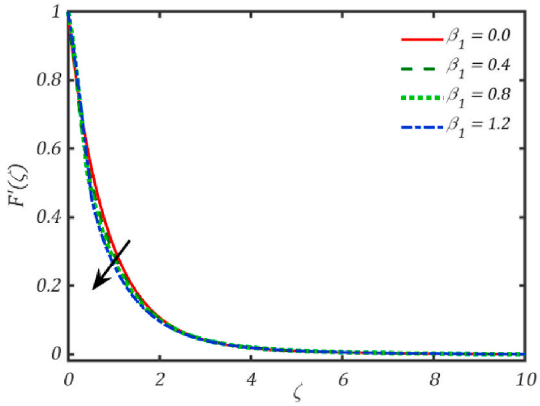


**Fig. 3.** Impression of $\beta_1$ on $F^{'}(\zeta)$.

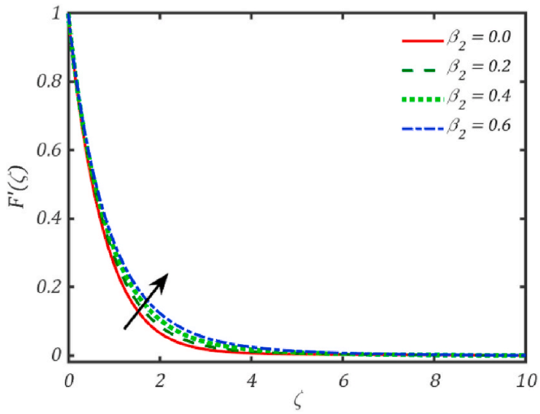


**Fig. 4.** Impression of $\beta_2$ on $F^{'}(\zeta)$.

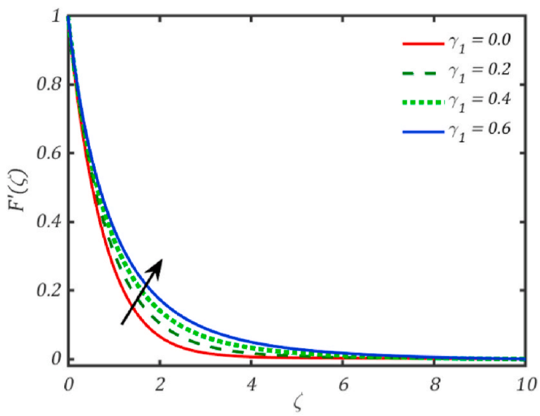


**Fig. 5.** Impression of $\gamma_1$ on $F^{'}(\zeta)$.

By raising the values of the Sutterby fluid factor, the heat transfer and friction force improved. The viscosity of liquid enhanced due to larger values of Sutterby fluid parameter ultimately declining the heat and friction near the surface. Heat transfer rate and friction force publicized improve due to different values of Sponginess parameter. Physically, the permeability of the porous material generates an increase in resistance, which boosts the values of friction between surface and fluid. The Darcy resistant parameter improved which declined the friction and movement of heat transfer. The magnetic field boosted up which declined the friction and movement of heat between surface and liquid. The induced magnetic field applied on the fluid which reduced heat transfer rate and friction forces. The

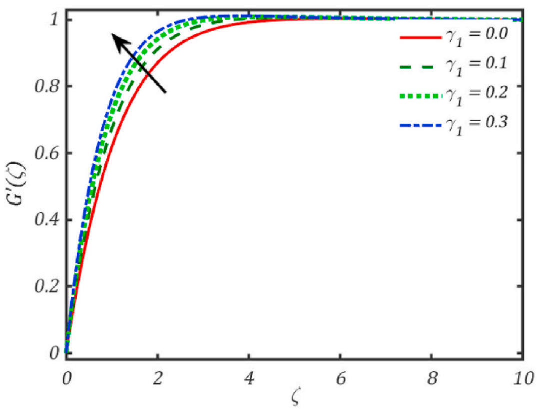


**Fig. 6.** Impression of $\gamma_1$ on $G^{'}(\zeta)$.

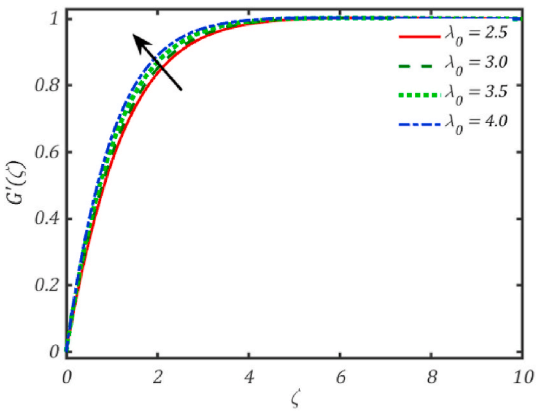


**Fig. 7.** Impression of $\lambda_0$ on $G^{'}(\zeta)$.

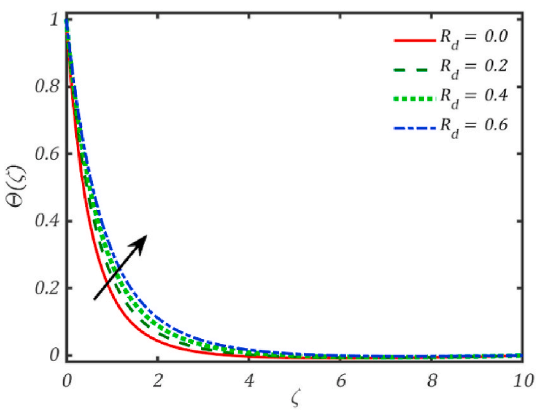


**Fig. 8.** Impression of $R_d$ on $\Theta(\zeta)$.

magnetic Prandtl number declined due to increasing values of movement of heat and friction. The heat transfer rate exposed lesser due to boost up value of radiation but friction between surface and liquid. Nusselt number revealed boost up for improving the values of Prandtl number while friction force remains fixed due to changes values of Prandtl number. Nusselt number exposed boost up for improving the values of Eckert number while friction force remains fixed due to changes values of Eckert factor. Dufour parameter improved gradually which declined heat transfer at cylindrical surface. Schmidt parameter improved gradually which declined heat transfer at cylindrical surface. Soret parameter improved gradually which enlarged heat transfer at the cylindrical surface. The nusselt number boosted while skin friction remained constant due to enlarging values of variable thermal conductivity. Table 2 shows the

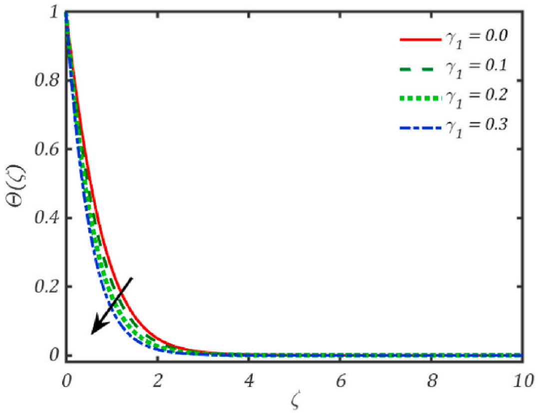


**Fig. 9.** Impression of $\gamma_1$ on $\Theta\zeta)$.

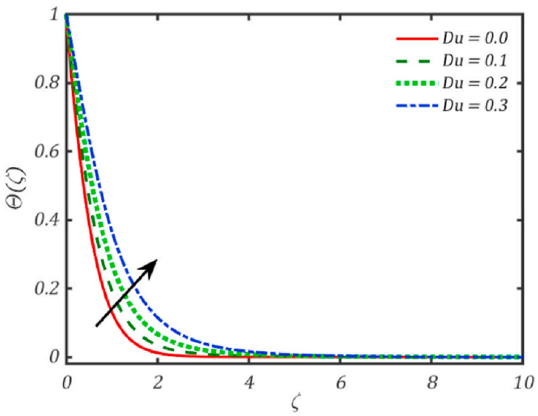


**Fig. 10.** Impression of $Du$ on $\Theta(\zeta)$.

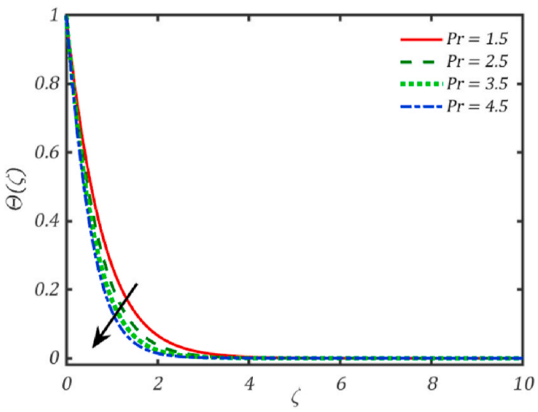


**Fig. 11.** Impression of $Pr$ on $\Theta(\zeta)$.

results of Rangi and Ahmad [51] compared with the actual results for various $\epsilon$ values for $\Theta^{'}(0)$ when the rest of the physical parameters are taken as zero. Note that our results are in good agreement with Rangi and Ahmad [51] when with $\beta_1 = \lambda_1 = \beta_2 = \beta = \lambda_0 = R_d = Ec = Du = Sr = Sc = 0$ and $Pr = 1.0$.

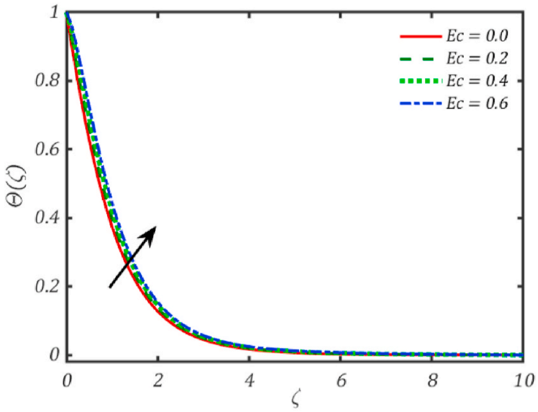


**Fig. 12.** Impression of *Ec* on $\Theta(\zeta)$.

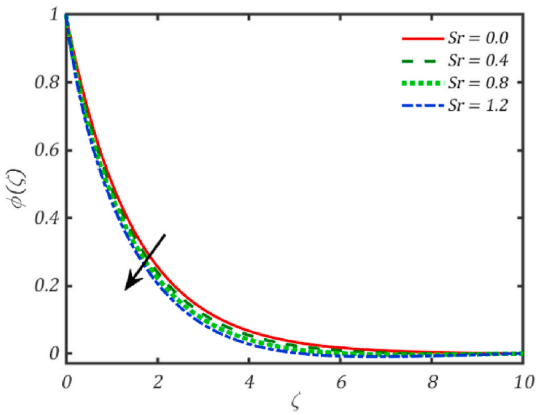


**Fig. 13.** Impression of *Sr* on $\varphi(\zeta)$.

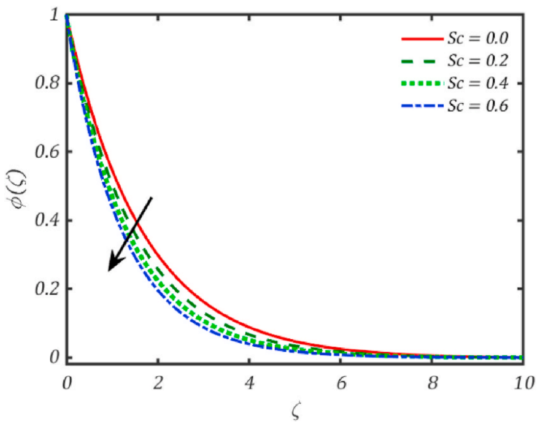


**Fig. 14.** Impression of *Sc* on $\varphi(\zeta)$.

## 5. Conclusion

Induced magnetic field sutterby fluid flow over a stretching cylinder is deliberated under Darcy resistance. Radiation and thermal slip are considered to debate the impact on the cylindrical surface. The Dufour and Soret impacts are considered on the cylinder. The main achievements are highlighted as follows:

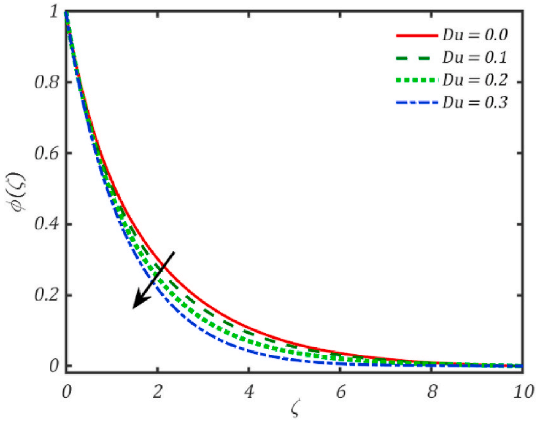


**Fig. 15.** Impression of *Du* on $\varphi(\zeta)$.

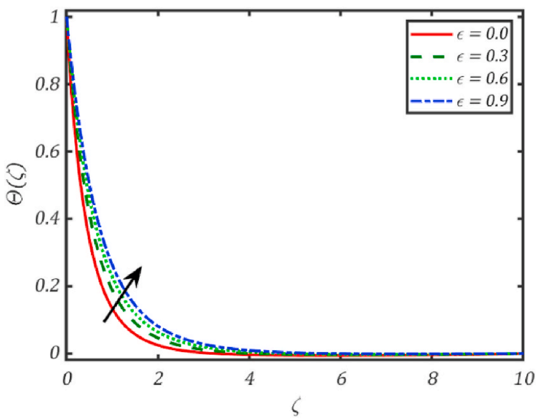


**Fig. 16.** Impression of $\epsilon$ on $\Theta(\zeta)$.

- The skin friction and Nusselt number revealed less values by an increment of curvature parameter. The curvature of the cylindrical surface expanded, which reduced heat transfer phenomena due to the large surface area covered. However, skin friction is reduced because of the increment in the curvature of the cylindrical surface; the surface becomes flat, and the friction force is reduced.
- The heat transfer and friction force improved by enlarging the values of the Sutterby fluid factor. The viscosity of liquid enhanced due to larger values of the Sutterby fluid factor ultimately upgrading the heat and friction near the surface.
- Heat transfer rate and friction force improved due to different values of Sponginess parameter. Physically, the permeability of the porous material generates an increase in resistance, which boosts the values of friction between fluid and surface.
- The Darcy resistant parameter improved, reducing the friction and movement of heat transfer. The magnetic field boosted up, which declined the friction and movement of heat between the surface and liquid.

## Data availability

No data was used for the research described in the article.


## Funding

No funding


## CRediT authorship contribution statement

**Nadeem Abbas:** Writing – review & editing, Writing – original draft, Methodology, Investigation, Conceptualization. **Zead Mustafa:** Writing – review & editing, Methodology, Data curation. **Kamaleldin Abodayeh:** Visualization, Validation. **Taqi A.M. Shatnawi:** Investigation, Formal analysis. **Wasfi Shatanawi:** Validation, Supervision, Software, Formal analysis.

**Table 1**
Nusselt number and Skin friction for various physical parameters.

| $\gamma_1$ | $\beta_1$ | $\lambda_1$ | $\beta_2$ | $\beta$ | $\lambda_0$ | $R_d$ | $Pr$ | $Ec$ | $Du$ | $Sc$ | $Sr$ | $\epsilon$ | $N_u{}^n$ | $C_f{}^S$ |
|---|---|---|---|---|---|---|---|---|---|---|---|---|---|---|
| 0.1 | 0.2 | 0.3 | 0.4 | 0.2 | 1.5 | 0.1 | 2.5 | 0.1 | 0.3 | 0.3 | 0.1 | 0.3 | 1.874262 | −1.861863 |
| 0.2 | – | – | – | – | – | – | – | – | – | – | – | – | 1.776790 | −1.200218 |
| 0.3 | – | – | – | – | – | – | – | – | – | – | – | – | 1.667783 | −1.191969 |
| 0.4 | – | – | – | – | – | – | – | – | – | – | – | – | 1.574710 | −1.167122 |
| 0.2 | 0.0 | – | – | – | – | – | – | – | – | – | – | – | 1.778245 | −1.070026 |
| – | 0.2 | – | – | – | – | – | – | – | – | – | – | – | 1.77679 | −1.200218 |
| – | 0.4 | – | – | – | – | – | – | – | – | – | – | – | 1.775119 | −1.338146 |
| – | 0.6 | – | – | – | – | – | – | – | – | – | – | – | 1.77313 | −1.489551 |
| – | 0.2 | 0.1 | – | – | – | – | – | – | – | – | – | – | 1.8949099 | −1.140464 |
| – | – | 0.3 | – | – | – | – | – | – | – | – | – | – | 1.7767900 | −1.200218 |
| – | – | 0.5 | – | – | – | – | – | – | – | – | – | – | 1.7497780 | −1.255118 |
| – | – | 0.7 | – | – | – | – | – | – | – | – | – | – | 1.7227960 | −1.309786 |
| – | – | 0.3 | 0.2 | – | – | – | – | – | – | – | – | – | 1.776342 | −1.20331 |
| – | – | – | 0.4 | – | – | – | – | – | – | – | – | – | 1.77679 | −1.200218 |
| – | – | – | 0.6 | – | – | – | – | – | – | – | – | – | 1.777237 | −1.197144 |
| – | – | – | 0.8 | – | – | – | – | – | – | – | – | – | 1.777683 | −1.194088 |
| – | – | – | 0.4 | 0.2 | – | – | – | – | – | – | – | – | 1.77679 | −1.200218 |
| – | – | – | – | 0.4 | – | – | – | – | – | – | – | – | 1.83809 | −1.130643 |
| – | – | – | – | 0.6 | – | – | – | – | – | – | – | – | 1.977124 | −0.9223671 |
| – | – | – | – | 0.8 | – | – | – | – | – | – | – | – | 2.17182 | −0.7605157 |
| – | – | – | – | 0.2 | 1.5 | – | – | – | – | – | – | – | 1.77679 | −1.200218 |
| – | – | – | – | – | 2.0 | – | – | – | – | – | – | – | 1.750116 | −1.228851 |
| – | – | – | – | – | 2.5 | – | – | – | – | – | – | – | 1.742192 | −1.237634 |
| – | – | – | – | – | 3.0 | – | – | – | – | – | – | – | 1.737946 | −1.240094 |
| – | – | – | – | – | 1.5 | 0.1 | – | – | – | – | – | – | 1.77679 | −1.200218 |
| – | – | – | – | – | – | 0.3 | – | – | – | – | – | – | 1.905318 | −1.200218 |
| – | – | – | – | – | – | 0.5 | – | – | – | – | – | – | 2.024203 | −1.200218 |
| – | – | – | – | – | – | 0.7 | – | – | – | – | – | – | 2.135149 | −1.200218 |
| – | – | – | – | – | – | 0.1 | 1.0 | – | – | – | – | – | 1.920884 | −1.200218 |
| – | – | – | – | – | – | – | 1.5 | – | – | – | – | – | 1.856346 | −1.200218 |
| – | – | – | – | – | – | – | 2.0 | – | – | – | – | – | 1.727922 | −1.200218 |
| – | – | – | – | – | – | – | 2.5 | – | – | – | – | – | 1.77679 | −1.200218 |
| – | – | – | – | – | – | – | 2.5 | 0.0 | – | – | – | – | 1.833323 | −1.200218 |
| – | – | – | – | – | – | – | – | 0.1 | – | – | – | – | 1.77679 | −1.200218 |
| – | – | – | – | – | – | – | – | 0.2 | – | – | – | – | 1.720333 | −1.200218 |
| – | – | – | – | – | – | – | – | 0.3 | – | – | – | – | 1.663952 | −1.200218 |
| – | – | – | – | – | – | – | – | 0.1 | 0.1 | – | – | – | 2.131304 | −1.200218 |
| – | – | – | – | – | – | – | – | – | 0.3 | – | – | – | 1.77679 | −1.200218 |
| – | – | – | – | – | – | – | – | – | 0.5 | – | – | – | 1.446937 | −1.200218 |
| – | – | – | – | – | – | – | – | – | 0.7 | – | – | – | 1.148901 | −1.200218 |
| – | – | – | – | – | – | – | – | – | 0.3 | 0.1 | – | – | 1.879545 | −1.200218 |
| – | – | – | – | – | – | – | – | – | – | 0.3 | – | – | 1.77679 | −1.200218 |
| – | – | – | – | – | – | – | – | – | – | 0.5 | – | – | 1.688214 | −1.200218 |
| – | – | – | – | – | – | – | – | – | – | 0.7 | – | – | 1.608465 | −1.200218 |
| – | – | – | – | – | – | – | – | – | – | 0.3 | 0.1 | – | 1.77679 | −1.200218 |
| – | – | – | – | – | – | – | – | – | – | – | 0.2 | – | 1.784157 | −1.200218 |
| – | – | – | – | – | – | – | – | – | – | – | 0.3 | – | 1.791611 | −1.200218 |
| – | – | – | – | – | – | – | – | – | – | – | 0.4 | – | 1.799154 | −1.200218 |
| – | – | – | – | – | – | – | – | – | – | – | 0.1 | 0.0 | 1.51928 | −1.200218 |
| – | – | – | – | – | – | – | – | – | – | – | – | 0.3 | 1.77679 | −1.200218 |
| – | – | – | – | – | – | – | – | – | – | – | – | 0.6 | 2.012539 | −1.200218 |
| – | – | – | – | – | – | – | – | – | – | – | – | 0.9 | 2.231421 | −1.200218 |

**Table 2**
Comparative outcomes of current analysis with Rangi and Ahmad [51] for various values of $\gamma_1$ with $\beta_1 = \lambda_1 = \beta_2 = \beta = \lambda_0 = R_d = Ec = Du = Sr = Sc = 0$ and $Pr = 1.0$.

| | Present results | | Rangi and Ahmad [51] | |
|---|---|---|---|---|
| $\gamma_1$ | $\epsilon = 0.0$ | $\epsilon = 0.2$ | $\epsilon = 0.0$ | $\epsilon = 0.2$ |
| 0.0 | −0.989453 | −0.8708143 | −0.985286 | −0.862122 |
| 0.25 | −1.087542 | −0.9512472 | −1.079447 | −0.949659 |
| 0.50 | −1.183420 | −1.0437821 | −1.173899 | −1.037605 |
| 0.75 | −1.272102 | −1.1312764 | −1.267214 | −1.124397 |
| 1.0 | −1.362015 | −1.2110952 | −1.359308 | −1.209949 |

## Declaration of competing interest

The authors declare no conflict of interest.


## Acknowledgment

The authors would like to thank Prince Sultan University for their support through the TAS research lab.


## References


[1] L.J. Crane, Boundary layer flow due to a stretching cylinder, Zeitschrift für angewandte Mathematik und Physik ZAMP 26 (5) (1975) 619–622.
[2] C.Y. Wang, Fluid flow due to a stretching cylinder, The Physics of fluids 31 (3) (1988) 466–468.
[3] M. Bourgoin, P. Odier, J.F. Pinton, Y. Ricard, An iterative study of time independent induction effects in magnetohydrodynamics, Physics of fluids 16 (7) (2004) 2529–2547.
[4] Y.S. Daniel, Steady MHD laminar flows and heat transfer adjacent to porous stretching sheets using HAM, American journal of heat and mass transfer 2 (3) (2015) 146–159.
[5] Y.S. Daniel, Laminar convective boundary layer slip flow over a flat plate using homotopy analysis method, J. Inst. Eng.: Series E 97 (2016) 115–121.
[6] Y.S. Daniel, MHD laminar flows and heat transfer adjacent to permeable stretching sheets with partial slip condition, Journal of Advanced Mechanical Engineering 4 (1) (2017) 1–15.
[7] Y.S. Daniel, Z.A. Aziz, Z. Ismail, F. Salah, Numerical study of entropy analysis for electrical unsteady natural magnetohydrodynamic flow of nanofluid and heat transfer, Chin. J. Phys. 55 (5) (2017) 1821–1848.
[8] R. Meenakumari, P. Lakshminarayana, K. Vajravelu, Influence of induced magnetic field and slip conditions on convective Prandtl fluid flow over a stretching surface with homogeneous and heterogeneous reactions, Multidiscip. Model. Mater. Struct. 17 (1) (2020) 127–147.
[9] M. Ramamoorthy, L. Pallavarapu, Radiation and Hall effects on a 3D flow of MHD Williamson fluid over a stretchable surface, Heat Transfer 49 (8) (2020) 4410–4426.
[10] G. Kotha, V.R. Kolipaula, M. Venkata Subba Rao, S. Penki, A.J. Chamkha, Internal heat generation on bioconvection of an MHD nanofluid flow due to gyrotactic microorganisms, The European Physical Journal Plus 135 (2020) 1–19.
[11] K. Gangadhar, A.J. Chamkha, Entropy minimization on magnetized Boussinesq couple stress fluid with non-uniform heat generation, Phys. Scripta 96 (9) (2021), 095205.
[12] R. Meenakumari, P. Lakshminarayana, MHD 3D flow of powell eyring fluid over a bidirectional nonlinear stretching surface with temperature dependent conductivity and heat absorption/generation, Proc. IME E J. Process Mech. Eng. 236 (6) (2022) 2580–2588.
[13] J. Sharma, A. Wakif, Comprehensive Analyses of Probable Influencing Factors Responsible for the Onset of Convective Instabilities in Various Viscous Fluidic Media Involving Metallic/non-Metallic Nanoparticles. Waves in Random and Complex Media, 2022, pp. 1–20.
[14] N. Abbas, K.U. Rehman, W. Shatanawi, A.A. Al-Eid, Theoretical study of non-Newtonian micropolar nanofluid flow over an exponentially stretching surface with free stream velocity, Adv. Mech. Eng. 14 (7) (2022), 16878132221107790.
[15] U. Manzoor, H. Waqas, T. Muhammad, A. Wakif, Oldroyd-B Nanofluid Flow with the Features of Bioconvection and Cattaneo-Christov Model in the Presence of Gyrotactic Motile Microorganism. Waves in Random and Complex Media, 2022, pp. 1–23.
[16] U. Khan, A. Zaib, A. Ishak, I. Waini, A. Wakif, A.M. Galal, Agrawal nanofluid flow towards a stagnation point past a moving disk with smoluchowski temperature and Maxwell velocity slip boundary conditions: the case of Buongiorno's model, ZAMM-Journal of Applied Mathematics and Mechanics/Zeitschrift für Angewandte Mathematik und Mechanik 103 (3) (2023), e202200051.
[17] M.S. Arif, K. Abodayeh, Y. Nawaz, Design of finite difference method and neural network approach for casson nanofluid flow: a computational study, Axioms 12 (6) (2023) 527.
[18] M.S. Arif, K. Abodayeh, Y. Nawaz, The modified finite element method for heat and mass transfer of unsteady reacting flow with mixed convection, Frontiers in Physics 10 (2022), 952787.
[19] Ishtiaq B.Nadeem S.Alzabut J.Effects of variable magnetic field and partial slips on the dynamics of Sutterby nanofluid due to biaxially exponential and nonlinear stretchable sheetsHeliyon972023.
[20] A. Gailitis, O. Lielausis, S. Dement'ev, E. Platacis, A. Cifersons, G. Gerbeth, G. Will, Detection of a flow induced magnetic field eigenmode in the Riga dynamo facility, Phys. Rev. Lett. 84 (19) (2000) 4365.
[21] K.S. Mekheimer, Effect of the induced magnetic field on peristaltic flow of a couple stress fluid, Phys. Lett. 372 (23) (2008) 4271–4278.
[22] Y.S. Daniel, Z.A. Aziz, Z. Ismail, F. Salah, Entropy analysis in electrical magnetohydrodynamic (MHD) flow of nanofluid with effects of thermal radiation, viscous dissipation, and chemical reaction, Theoretical and Applied Mechanics Letters 7 (4) (2017) 235–242.
[23] Y.S. Daniel, Z.A. Aziz, Z. Ismail, F. Salah, Double stratification effects on unsteady electrical MHD mixed convection flow of nanofluid with viscous dissipation and Joule heating, J. Appl. Res. Technol. 15 (5) (2017) 464–476.
[24] Y.S. Daniel, MHD laminar flows and heat transfer adjacent to permeable stretching sheets with partial slip condition, Journal of Advanced Mechanical Engineering 4 (1) (2017) 1–15.
[25] Y.S. Daniel, Z.A. Aziz, Z. Ismail, F. Salah, Entropy analysis of unsteady magnetohydrodynamic nanofluid over stretching sheet with electric field, Int. J. Multiscale Comput. Eng. 15 (6) (2017).
[26] Y.S. Daniel, Z.A. Aziz, Z. Ismail, A. Bahar, F. Salah, Stratified electromagnetohydrodynamic flow of nanofluid supporting convective role, Kor. J. Chem. Eng. 36 (2019) 1021–1032.
[27] Y.S. Daniel, Z.A. Aziz, Z. Ismail, F. Salah, Hydromagnetic slip flow of nanofluid with thermal stratification and convective heating, Aust. J. Mech. Eng. 18 (2) (2020) 147–155.
[28] V.R. Mulinti, L. Pallavarapu, Influence of thermal radiation and viscous dissipation on MHD flow of UCM fluid over a porous stretching sheet with higher order chemical reaction, Spec. Top Rev. Porous Media Int. J. 12 (4) (2021).
[29] A. Wakif, A. Abderrahmane, K. Guedri, B. Bouallegue, R. Kaewthongrach, P. Kaewmesri, A. Jirawattanapanit, Importance of exponentially falling variability in heat generation on chemically reactive von kármán nanofluid flows subjected to a radial magnetic field and controlled locally by zero mass flux and convective heating conditions: a differential quadrature analysis, Frontiers in Physics 768 (2022).
[30] Vinodkumar M. Reddy, P. Lakshminarayana, Higher order chemical reaction and radiation effects on magnetohydrodynamic flow of a maxwell nanofluid with Cattaneo–Christov heat flux model over a stretching sheet in a porous medium, J. Fluid Eng. 144 (4) (2022), 041204.
[31] S.D. Yahaya, U. Aliyu, H. Umaru, Stagnation point flow with thermal and magnetic field over a stretching sheet, Sci. World J. 17 (2) (2022) 191–199.
[32] U.S. Mahabaleshwar, K.N. Sneha, A. Wakif, Significance of Thermo-Diffusion and Chemical Reaction on MHD Casson Fluid Flows Conveying CNTs over a Porous Stretching Sheet. Waves in Random and Complex Media, 2023, pp. 1–19.
[33] M.I. Anwar, H. Firdous, A.A. Zubaidi, N. Abbas, S. Nadeem, Computational analysis of induced magnetohydrodynamic non-Newtonian nanofluid flow over nonlinear stretching sheet, Prog. React. Kinet. Mech. 47 (2022), 14686783211072712.
[34] H.T. Alkasasbeh, A. Abderrahmane, A. Mourad, K. Guedri, E.M. Tag, O. Younis, Analysis of 3-D MHD maxwell hybrid nanofluid flow over a stretching sheet, Heliyon (2023), 4376147, https://doi.org/10.2139/ssrn.4376147, pp. 1-23. Available at: SSRN.

[35] S. Zeb, S. Gul, K. Shah, D. Santina, N. Mlaiki, Melting heat transfer and thermal radiation effects on MHD tangent hyperbolic nanofluid flow with chemical reaction and activation energy, Therm. Sci. 27 (Spec. issue 1) (2023) 253–261.
[36] N. Elboughdiri, D. Ghernaout, T. Muhammad, A. Alshehri, R. Sadat, M.R. Ali, A. Wakif, Towards a novel EMHD dissipative stagnation point flow model for radiating copper-based ethylene glycol nanofluids: an unsteady two-dimensional homogeneous second-grade flow case study, Case Stud. Therm. Eng. 45 (2023), 102914.
[37] Y.S. Daniel, S.K. Daniel, Effects of buoyancy and thermal radiation on MHD flow over a stretching porous sheet using homotopy analysis method, Alex. Eng. J. 54 (3) (2015) 705–712.
[38] Y.S. Daniel, Z.A. Aziz, Z. Ismail, F. Salah, Slip effects on electrical unsteady MHD natural convection flow of nanofluid over a permeable shrinking sheet with thermal radiation, Eng. Lett. 26 (1) (2018).
[39] Y.S. Daniel, Z.A. Aziz, Z. Ismail, F. Salah, Impact of thermal radiation on electrical MHD flow of nanofluid over nonlinear stretching sheet with variable thickness, Alex. Eng. J. 57 (3) (2018) 2187–2197.
[40] Y.S. Daniel, Z.A. Aziz, Z. Ismail, F. Salah, Thermal stratification effects on MHD radiative flow of nanofluid over nonlinear stretching sheet with variable thickness, Journal of Computational Design and Engineering 5 (2) (2018) 232–242.
[41] Y.S. Daniel, Z.A. Aziz, Z. Ismail, A. Bahar, F. Salah, Slip role for unsteady MHD mixed convection of nanofluid over stretching sheet with thermal radiation and electric field, Indian J. Phys. 94 (2020) 195–207.
[42] K. Gangadhar, M.A. Kumari, A.J. Chamkha, EMHD flow of radiative second-grade nanofluid over a Riga Plate due to convective heating: revised Buongiorno's nanofluid model, Arabian J. Sci. Eng. 47 (7) (2022) 8093–8103.
[43] M.V. Reddy, P. Lakshminarayana, MHD radiative flow of Williamson nanofluid with Cattaneo-Christov model over a stretching sheet through a porous medium in the presence of chemical reaction and suction/injection, J. Porous Media (2022) 25.
[44] K. Gangadhar, R. Edukondala Nayak, M. Venkata Subba Rao, A.J. Chamkha, Nonlinear radiations in chemically reactive Walter's B nanoliquid flow through a rotating cone, Proc. IME E J. Process Mech. Eng. (2022), 09544089221105932.
[45] D.N. Bhargavi, K. Gangadhar, A.J. Chamkha, Graphene-gold/PDMS Maxwell hybrid nanofluidic flow in a squeezed channel with linear and irregular radiations, Proc. IME E J. Process Mech. Eng. (2022), 09544089221139696.
[46] K. Gangadhar, E. Mary Victoria, A.J. Chamkha, Hydrothermal features in the swirling flow of radiated graphene–Fe3O4 hybrid nanofluids through a rotating cylinder with exponential space-dependent heat generation, Waves Random Complex Media (2022) 1–24.
[47] K. Gangadhar, P. Manasa Seshakumari, M. Venkata Subba Rao, A.J. Chamkha, Biconvective transport of magnetized couple stress fluid over a radiative paraboloid of revolution, Proc. IME E J. Process Mech. Eng. 236 (4) (2022) 1661–1670.
[48] A. Wakif, Numerical inspection of two-dimensional MHD mixed bioconvective flows of radiating Maxwell nanofluids nearby a convectively heated vertical surface, Waves Random Complex Media (2023) 1–22.
[49] K. Gangadhar, M. Prameela, A.J. Chamkha, Exponential space-dependent heat generation on Powell–Eyring hybrid nanoliquid under nonlinear thermal radiation, Indian J. Phys. (2023) 1–13.
[50] S. Khan, M.M. Selim, A. Khan, A. Ullah, T. Abdeljawad, . Ikramullah, W.K. Mashwani, On the analysis of the non-Newtonian fluid flow past a stretching/shrinking permeable surface with heat and mass transfer, Coatings 11 (5) (2021) 566.
[51] R.R. Rangi, N. Ahmad, Boundary Layer Flow Past a Stretching Cylinder and Heat Transfer with Variable Thermal Conductivity, 2012.